Journal of Environmental Economics & Chemical Processes (JEECP)

https://doi.org/10.22034/jeecp.2026.2087997.1016

Journal Homepage: *WWW.JEECPJournal.com*

Journal of Environmental Economics & Chemical Processes (JEECP)

ORIGINAL RESEARCH PAPER

Experimental, Theoretical and Application Studies of $(Ph_3P)3RhI$ and $(Et_3P)3RhI$ Catalysts in the Monsanto Process

Asadollah Farhadi [a,*]; Mohammad Shareei [b,*]; Reza Mosayebi Behbahani [b]; Omolbanin Hosseinkhani [c]; Seham Nasseri [a]

[a] *Department of Basic Sciences, Petroleum University of Technology, Abadan, Iran.*
[b] *Department of Gas Engineering, Petroleum University of Technology (PUT), Abadan, Iran.*
[c] *Department of Chemical Engineering, Amirkabir University of Technology (Tehran Polytechnic), Tehran, Iran.*

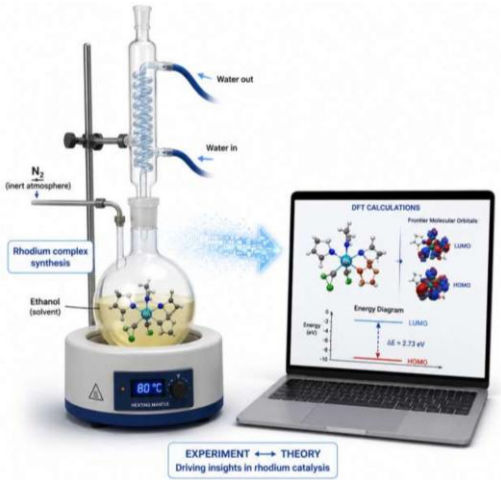
PAPER INFO

Paper history:
Received: 05/28/2026
Revised: 06/14/2026
Accepted in revised form: 06/17/2026
Published: 06/30/2026

Keywords:
Monsanto Process;
Acetic Acid;
$(Ph_3P)_3RhI$;
$(Et_3P)_3RhI$;
Density Functional Theory Method.

ABSTRACT

Acetic acid is efficiently produced via the carbonylation of methanol in the presence of iodomethane and carbon monoxide under various catalytic system and reaction conditions. In the Monsanto process, RhI_3 is employed as the catalyst for the effective synthesis of acetic acid. In this study, the synthesis of $(Ph_3P)_3RhI$ and $(Et_3P)_3RhI$ catalysts for acetic acid production is described. The differences in the electronic energy levels of these two complexes may influence their catalytic performance in acetic acid formation. Experimental data obtained under conditions identical to those of the Monsanto process, indicate that $(Et_3P)_3RhI$ exhibits superior catalytic performance compared to the other catalysts. The catalysts, were characterized using various spectroscopy techniques. In addition, their solubility under Monsanto process conditions was investigated. The solubility results revealed that after 6 and 20 hours, the solubility order of the catalysts was $(Ph_3P)_3RhI$>$(Et_3P)_3RhI$>RhI_3, respectively. Furthermore, their catalytic activities were evaluated using the density functional theory method. The results demonstrate that both phosphine-modified catalysts exhibit higher activity than RhI_3.



1. Introduction

Rhodium derivatives are among the most common catalysts used in laboratory reactions and industrial processes. They are employed in hydrogenation, hydroformylation, hydroboration and hydrosilylation of alkene [1]. Additionally, these complexes are used for methylation and alkylation via C–H functionalization, as well as for the polymerization of monosubstituted acetylene [2,3]. Derivative of these catalysts are also used in the industrial synthesis of acetic acid (AA) [4].

Several methods have been developed for the production of the AA. The Synthesis of acetic acid involves diverse catalysts and reaction pathways, each with distinct advantages and limitations. Currently, AA is synthesized via the conversion of CO_2 and hydrogen at the present, Rhodium catalyst [5-8]. It can also be produced form various feedstocks using different catalysts systems [9]. Furthermore, AA is industrially produced using an iridium-based catalyst through Cativa process [10].

*Corresponding Author: Asadollah Farhadi
E-mail address: farhadichem@put.ac.ir
ISSN: 3116-0050
URL: https://www.jeecpjournal.com/article_735331.html

Please cite this article as: A. Farhadi, M. Shareei, R. Mosayebi Behbahani, O. Hosseinkhani, S. Nasseri, *Journal of Enviromental Economics & Chemical Processes (JEECP)*, 2026, 3(2), 87-93. https://doi.org/10.22034/jeecp.2026.2087997.1016

/© 2026 The Author(s). Published by Power of New Vision Movement Institute.

Also, the Monsanto process is an industrial method for the generation of acetic acid by the catalytic carbonylation of methanol. This process is carried out by reaction of methanol with carbon monoxide in the presence of a $RhI_3.3H_2O$ catalyst to produce acetic acid [11].

One of the most significant applications of Rhodium derivatives in homogenous and heterogenous forms is the carbonylation of methanol to produce acetic acid. This reaction proceeds via the mechanism of the Monsanto process. In this reaction, methanol reacts with carbon monoxide in the presence of a rhodium catalyst to generate acetic acid [12].

Acetic acid industrial synthesis involves various pathways, such as

1. Methanol Hydrocarboxylation with CO_2 and H_2
2. Oxidation of Acetaldehyde
3. Carbonylation of Methanol
4. Anaerobic Fermentation

So, each method has advantages and limitations. The quest for sustainable and efficient methods continues to drive innovation in synthetic chemistry and chemical engineering. However, industrially, the most widely used method is the Monsanto process, which involves the carbonylation of methanol [13].

However, in this study, the synthesis of two homogeneous catalysts used in the Monsanto process is reported. Furthermore, their structures were investigated using the DFT method. In addition, the solubility of three catalysts in synthesis of acetic acid under the similar condition to those of the Monsanto process is reported in this work.

2. Experimental

2.1. Materials

$RhI_3.3H_2O$, triphenyl phosphine, triethylphosphine, benzene, diethyl ether, methanol and ethanol were purchased from Sigma-Aldrich chemical company. All materials were used without further purification.

2.2. Equipment

Melting points were determined using a Melting point Meter M3000 apparatus and were uncorrected. The FT-IR spectrum was recorded from KBr discs using a Bruker ALPHA FTIR spectrometer. The ^{1}HNMR spectrum was recorded using a Bruker Ascend 300 NMR spectrometer. The morphology of the particle was analyzed a field emission scanning electron microscope (FESEM TESCAN MIRA2). Thermogravimetric analysis (TGA) was carried out under nitrogen gas over a temperature range of 25-1000 °C at a heating rate of 5 °C.min^{-1} using a TGA STA6000 apparatus. The zeta spectrum was recorded using Malvern Instruments apparatus. The XRD spectrum was obtained using an XRD Philips PW1730 apparatus.

2.3. Synthesis of $(Ph_3P)_3RhI$

In a three-necked flask equipment with a condenser, 0.5 g (0.997 ×10^{-3} mol) of $RhI_3.3H_2O$ and 3 g (0.0458 mol) of Ph_3P were mixed in 70 mL of ethanol as solvent. The mixture was refluxed under an N_2 atmosphere for 6 h. The crude product was purified by benzene and ethanol. The black solid was then dried in an oven at 90 °C. The weight of the product was 0.65 g (0.639 ×10^{-3} mol) [14,15] (Scheme 1).

$$RhI_3.3H_2O + Ph_3P \xrightarrow[N_2,\ reflux]{Ethanol} (Ph_3P)_3RhI + Ph_3PO + HI$$

Scheme 1. Synthesis of $(Ph_3P)3RhI$

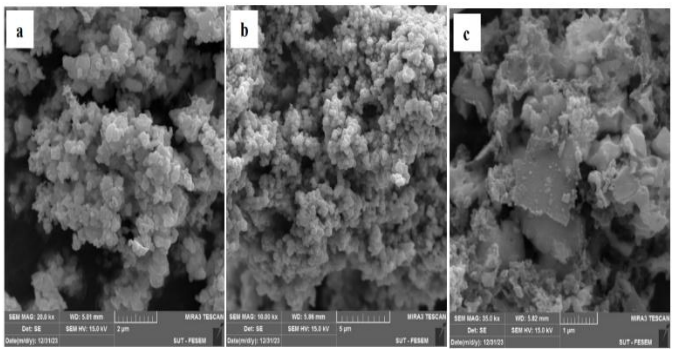


Figure 1. FE-SEM of a) $(Ph_3P)_3RhI$, b) $(Et_3P)_3RhI$, and c) $RhI_3.3H_2O$

2.4. Synthesis of $(Et_3P)_3RhI$

In a three-necked flask equipment with a condenser, 0.5 g (0.997 ×10^{-3} mol) of $RhI_3.3H_2O$ and 3 g (0.0254 mol) of Et_3P were mixed in 70 mL of ethanol as solvent. The mixture was refluxed under an N_2 atmosphere for 6 h. The crude product was purified by benzene and ethanol. The black solid was then dried in an oven at 90 °C. The weight of the product was 0.3 g (0.513 ×10^{-3} mol) [14,15].

2.5. Characterization

Two catalysts were characterized by melting point, FT-IR, ^{1}H-NMR, FE-SEM, EDX, XRD and Zeta potential.

The characterization of $(Ph_3P)_3RhI$ (m.p.= 218-223 °C) and $(Et_3P)_3RhI$ (m.p.= 214-217 °C) catalysts is reported below.

FT-IR $\bar{\upsilon}$ (cm^{-1}) spectra:

Figure 1 a and c show the comparison of the infrared spectra of $(Ph_3P)_3RhI$ and $RhI_3.3H_2O$. The appearance of a new band at 783 cm^{-1}; attributed to $\bar{\upsilon}$ (Rh-P), also confirms the coordination of the phosphorus atom to a metal center. In the $(Ph_3P)_3RhI$ complex, the decrease in the intensity of bands due to phosphine at 400-600 and 100-1100 cm^{-1} indicates that one phosphine molecule has been displaced during the coordination of the rhodium atom. In addition, the band observed at 2346 cm^{-1} is attributed to the benzene ring.

Figure 1 b and c show the evaluation of the infrared spectra of $(Et_3P)_3RhI$ and $RhI_3.3H_2O$. These data are similar to infrared spectra of $(Ph_3P)_3RhI$.

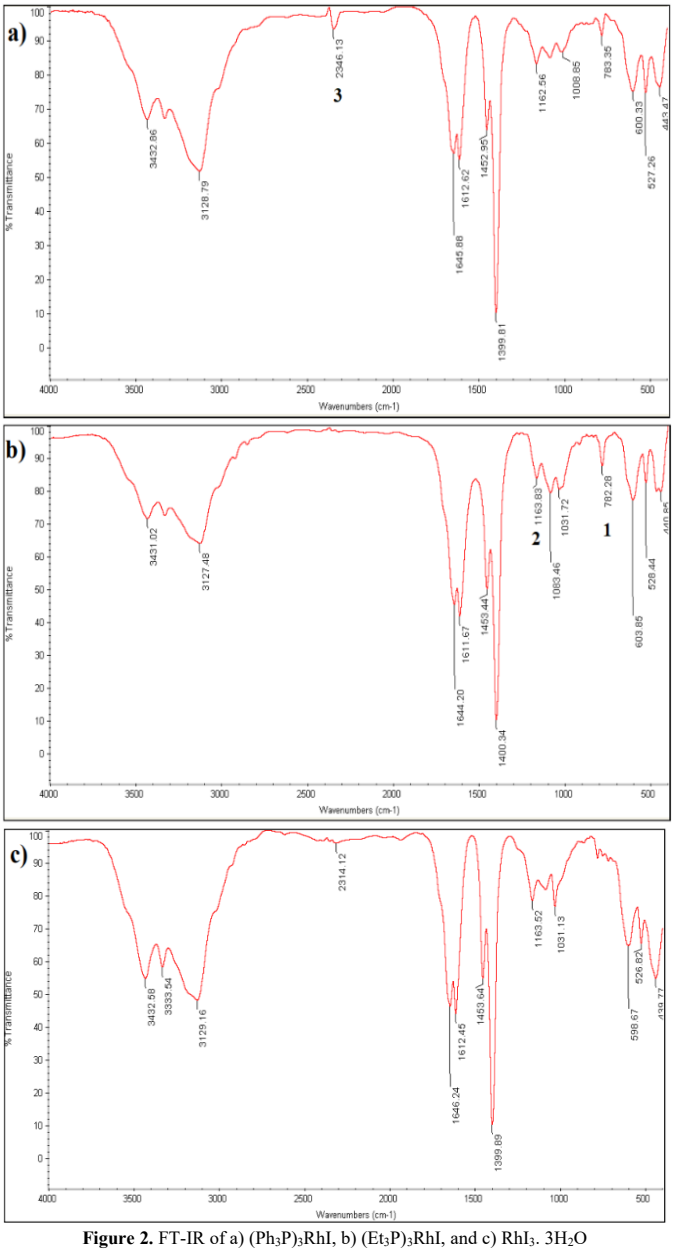


Figure 2. FT-IR of a) $(Ph_3P)_3RhI$, b) $(Et_3P)_3RhI$, and c) $RhI_3.3H_2O$

^{1}H-NMR spectra:

^{1}H-NMR (300 MHz) spectra were recorded on a Bruker instrument using DMSO-d_6 as solvent. ^{1}H chemical shifts are reported in ppm relative to TMS (Figure 2).

Rh $(Ph_3P)_3$: δ (ppm): 7.16-7.60 (H aromatic).

Rh $(Et_3P)_3$: δ (ppm): 0.92-1.88 (CH_3), 2.25-2.35 (CH_2).

RhI_3: δ (ppm): without peaks.

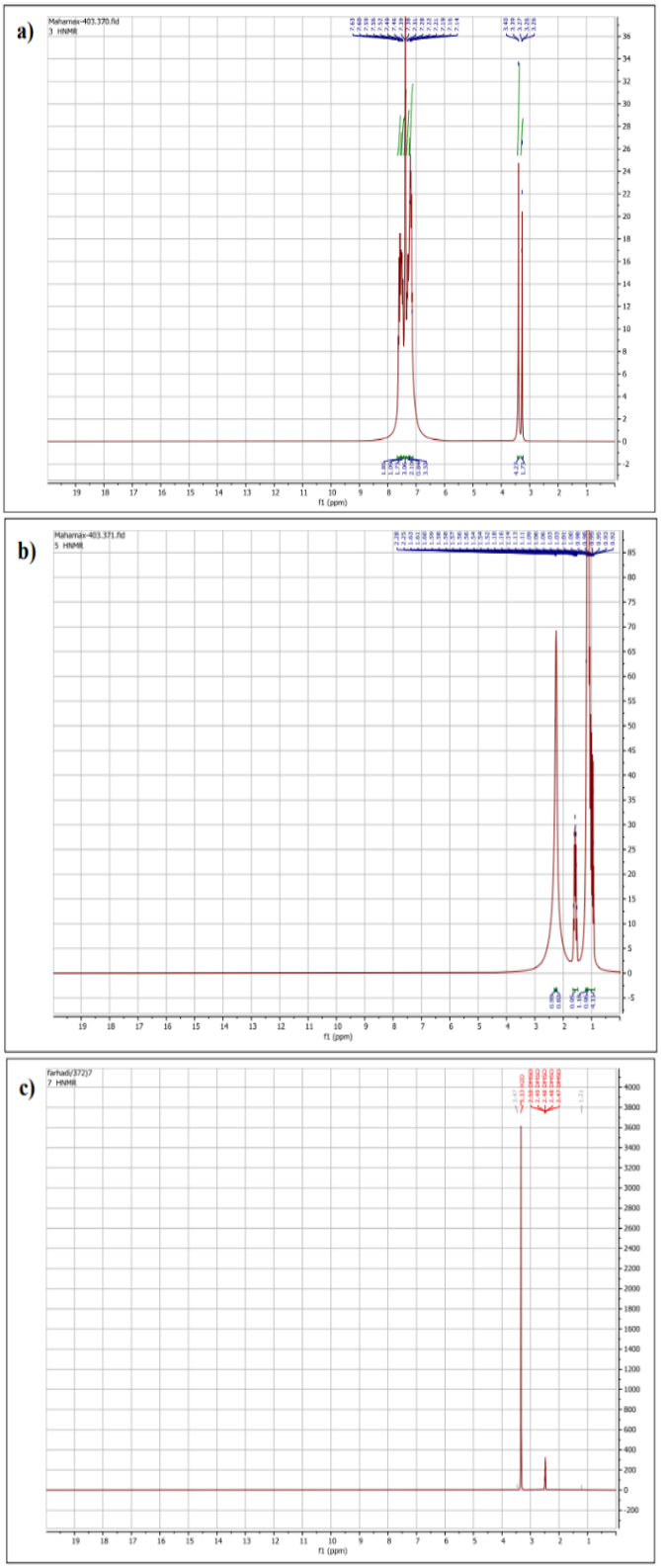


Figure 3. ^{1}HNMR of a) $(Ph_3P)_3RhI$ and b) $(Et_3P)_3RhI$ c) RhI_3. $3H_2O$

XRD pattern:

Figure 3 shows the XRD patterns of $(Ph_3P)_3RhI$ and $(Et_3P)_3RhI$ nanoparticles, which confirms their formation. The peaks were matched with the RhI_3 of file number ‘‘PDF # 045034” [16].

The X-ray diffraction (XRD) pattern of RhI_3 exhibits well-defined diffraction peaks, confirming the formation of a crystalline layered phase. The prominent reflections are observed at approximately 2θ ≈ 12–13°, 25°, 28–30°, 33–35°, and 40–42°.

Inaddition, well-defined diffraction peaks for $(Ph_3P)_3RhI$ appear in the XRD pattern at 2θ ≈ 8–10°, 10–12°, 13–14°, 21–22°, 24–25°, and 28–30°. These reflections confirm the crystalline nature of the compound. The absence of additional impurity peaks indicates that the synthesized $(Ph_3P)_3RhI$ possesses high phase purity and good crystallinity.

Similarly, the XRD pattern of $(Et_3P)_3RhI$ exhibits well-diffraction peaks at 2θ ≈8-10 °, 10-12 °, 12-13 °, and 13-14 °. These results demonstrate the successful synthesis and crystalline nature of this compound.

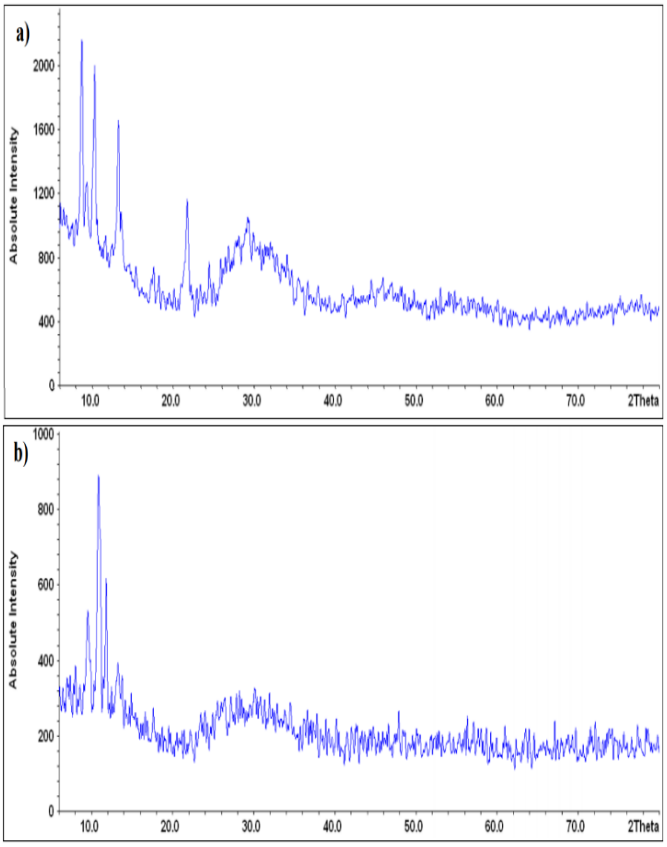


Figure 4. XRD pattern of a and b compounds.

FE-SEM analysis

FE-SEM image analysis is relatively suitable for investigating surface morphology and particle size/shape. Figure 4 (a) shows the FE-SEM image of a sphere-shaped but partially aggregated $(Ph_3P)_3RhI$ particles with a narrow size distribution, and the average particle size is in the range of 200nm-5µm. Figure 4 (b) shows the image of a sphere-shaped $(Et_3P)_3RhI$ particle. The average size of this composite is also in the range of 200 nm-5µm. Comparing images, a and b shows that the aggregated with a narrow size distribution in image b image is less than in image a. Comparing the morphology of pure RhI_3. $3H_2O$ with images a and b shows that the particles are more aggregated than in the other two images, therefore, this compound is flatter

EDX data:

The synthesized particles a) $(Ph_3P)_3RhI$ and b) $(Et_3P)_3RhI$ were also characterized by the energy dispersive X-ray (EDX) spectroscopy. Figure 5, shows the EDX spectra of a) $(Ph_3P)_3RhI$, b) $(Et_3P)_3RhI$, and c) the RhI_3 composite, respectively. The corresponding atomic compositions are:

57.5% C, 11.2% O, 9.6% P, 14.0%I, and 7.68% Rh in $(Ph_3P)_3RhI$;
31.6% C, 14.6% O, 12.8% P, 28.7%I, and 12.3% Rh in $(Et_3P)_3RhI$;
16.4% C, 22.2% O, 4.2% P, 39.8%I, and 17.4%% Rh in RhI_3 composite.

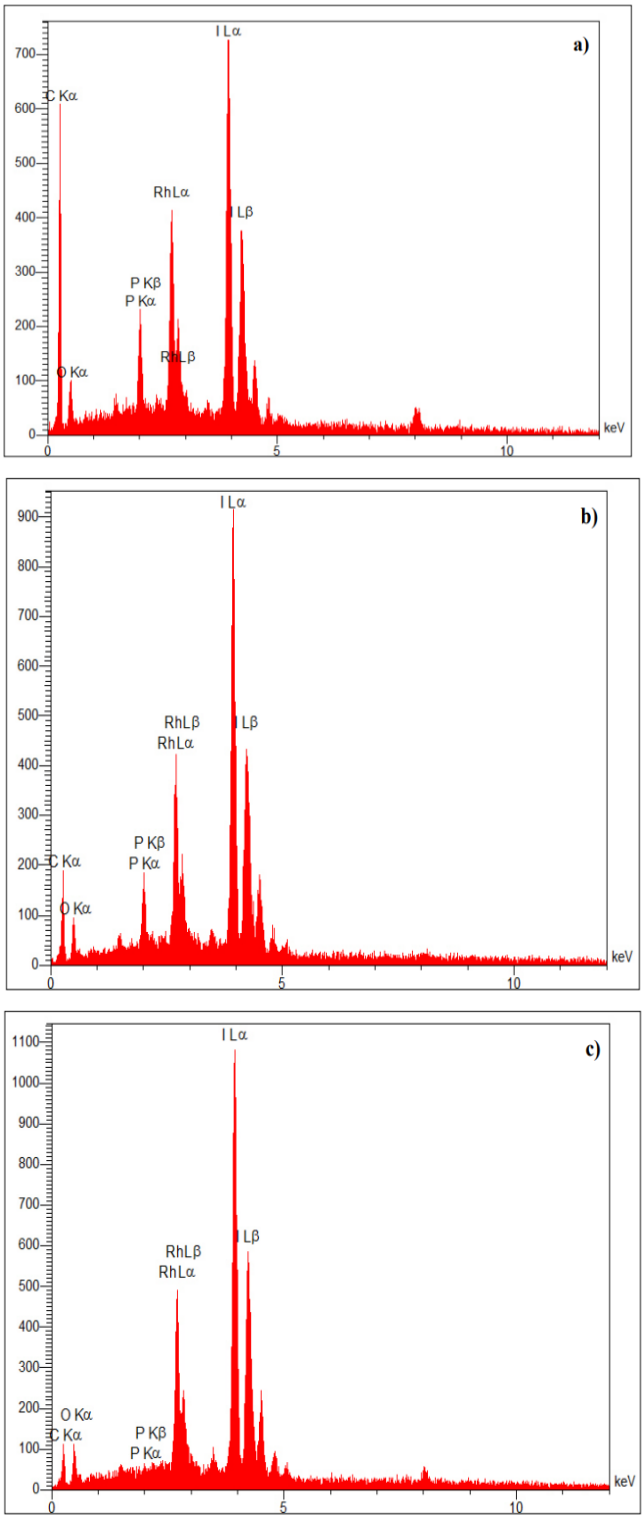


Figure 5. EDX survey spectra of a) $(Ph_3P)_3RhI$, b) $(Et_3P)_3RhI$, and c) RhI_3.

The analysis data show the formation of composites a and b as the percentages of C and P elements increase compared to compound c.

Thermogravimetric analysis (TGA)

Figure 6 shows the TGA results obtained for $(Ph_3P)_3RhI$, $(Et_3P)_3RhI$ and RhI_3. The plot shows the percentage mass as a function of sample temperature for three catalysts under a nitrogen purge.

The TGA data for three catalysts listed in Table 1, corresponding spectra are shown in Figure 6. The results indicate that the maximum weight loss due to thermal degradation for catalysts a, b, and c occurs at 546.53, 585.53, and 578.24 °C, respectively. All catalysts remain stable up to 970 °C.

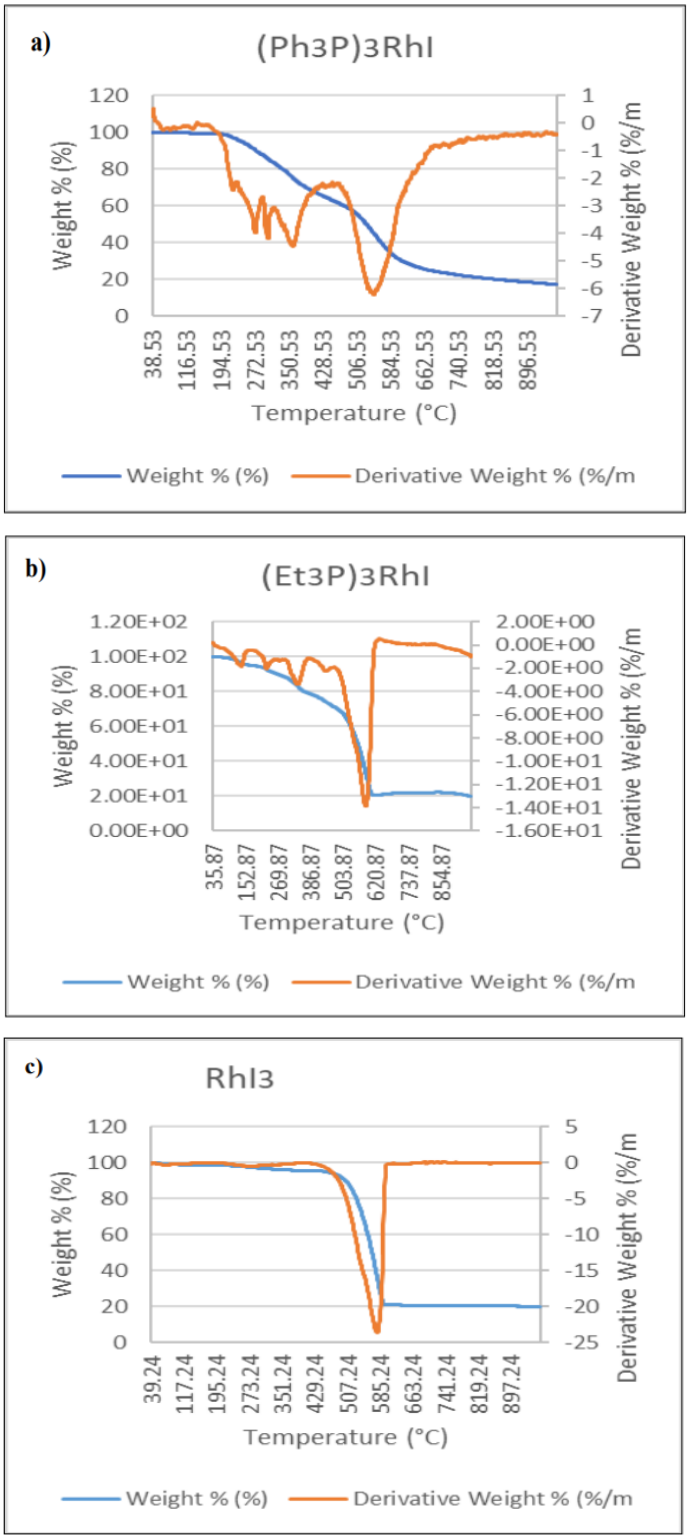


Figure 6. shown the TG spectra of a, b, and c catalysts.

Table 1. Thermal properties of $(Ph_3P)3RhI$, $(Et_3P)_3RhI$, and RhI_3 catalysts.

Comp.	CR[a]	T (°C)[b]	Time (mine)[c]
$(Ph_3P)_3$ RhI	6.18	546.53	45.25
$(Et_3P)_3$ RhI	13.88	585.53	29.07
RhI_3	23.60	578.24	28.46

a. Percentage weight of material left undecomposed after TGA analysis at maximum temperature in a nitrogen atmosphere.
b. Temperature at which maximum weight loss was recorded by TGA.
c. It is the time at which maximum weight loss.

Zeta potential analysis:

One of the methods for the characterization of compounds is the measurement of surface charge. Zeta potential is a method used to evaluate the surface of

charge in the colloidal system. The zeta potential data depends on the surface charge. This parameter is important for the stability of particles in suspension. Also, it is a major factor in the initial adsorption or coupling of particles to each other [17-19]. Thus, in this study, the zeta potential of compounds a, b, and c was measured (Figure 7). The particles showed frequency peaks of approximately -112, -90, and -28 mV for a, b, and c, respectively.

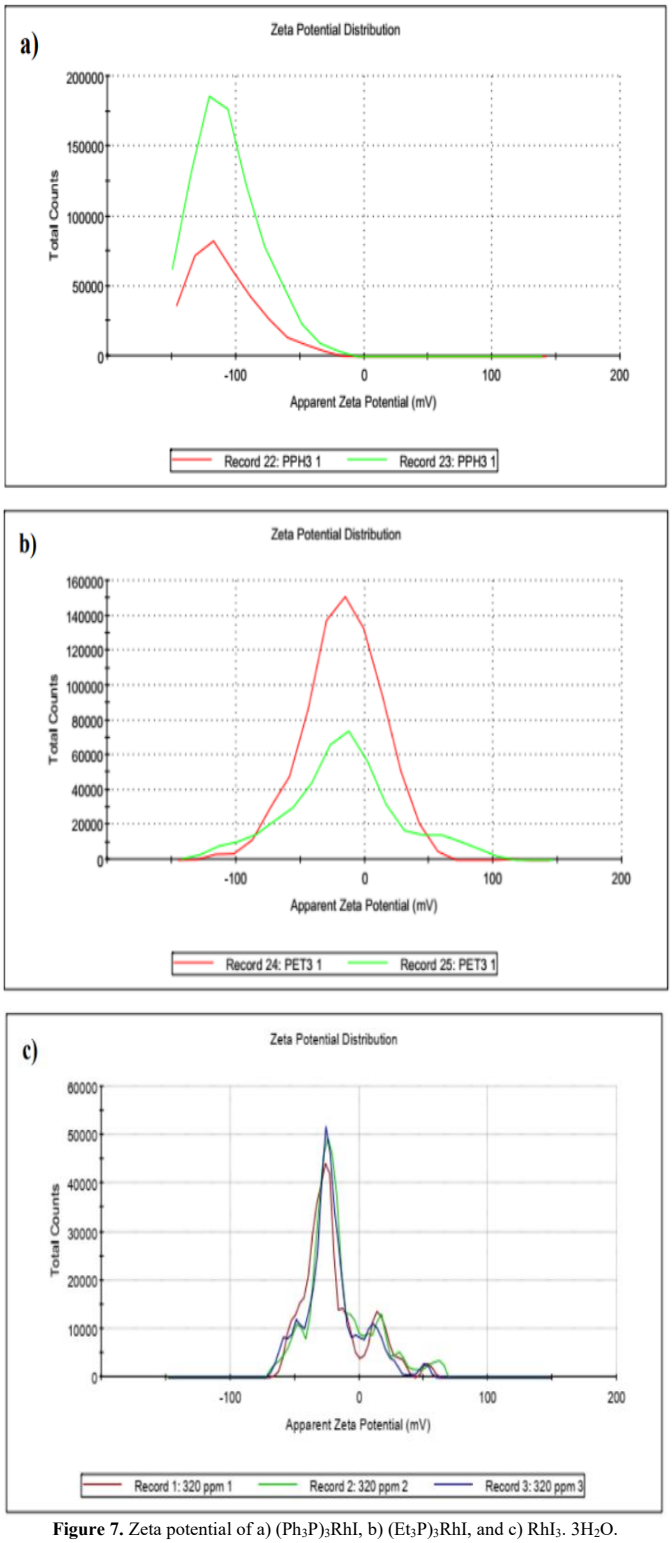


Figure 7. Zeta potential of a) $(Ph_3P)_3RhI$, b) $(Et_3P)_3RhI$, and c) RhI_3. $3H_2O$.

3. Synthesis of acetic acid via Monsanto process using RhI_3, (Ph3P)3RhI and $(Et_3P)3RhI$ as catalysts

According to the Monsanto process, the activity of two catalysts under the following conditions was investigated (Scheme 2). The reaction was carried out in a stainless-steel reactor with capacity of 1 L.

$$CO(g) + CH_3OH\ (l) + CH_3I\ (l) + H_2O\ (l) \xrightarrow[T/P]{\text{catalyst}} CH_3CO_2H + HI + \text{other by-products}$$

Scheme 2. synthesis of acetic acid by used three catalysts under the Monsanto process conditions.

According to the feedstocks reported in Table 2, the solubility of three catalysts was tested under different conditions.

Table 2. Feedstock were used for the solubility of three catalysts

Feedstock	HI	CH_3I	CH_3OH	H_2O	CH_3CO_2H
Percent	8.00	9.13	6.70	22.00	54.17

Table 3. The solubility of three catalysts under the condition in Table 2

Catalyst	RhI_3		$(Ph_3P)_3RhI$		$(Et_3P)_3RhI$	
Solubility (ppm)	40	86	64.1	138	38.5	125
Time (h)	6	20	6	20	6	20

At 120 ºC and a CO(g) pressure of 5 bar, and according to the data reported in Table 2, the solubility of the three catalysts is reported below (Table 3).

These data show that the solubility of three catalysts dependent on reaction time and the type of ligands. Thus, increasing reaction time leads to increase the solubility of these compounds. According to Table 3, the solubility of three catalysts at 120 °C is exothermic due to the increase in temperature during the reaction. Furthermore, replacing the iodine ligand with phosphine ligand derivatives changes the polarity of these compounds, ultimately leading to an increase in their solubility.

In this project, the feedstock mentioned in Table 4 were used for the synthesis of acetic acid. The progress of the reaction was monitored by gas chromatography (Table 5).

Table4. The feedstock used in this project.

Feedstock	HI	CH_3I	CH_3OH	H_2O
% Comp.	8.96	9.13	6.73	22

Table 5. Synthesis of acetic acid with RhI3, (Ph3P)3RhI, and (Et3P)3RhI at P=28 bar at T=120 ºC in a stainless-steel reactor (1 L). Acetic acid and Methyl acetate are denoted by AA and MAc, respectively.

Time (h)	RhI_3		$(Ph_3P)_3RhI$		$(Et_3P)_3RhI$	
%Product	%AA	%MAc	%AA	%MAc	%AA	%MAc
6	39.6	5.02	44.35	3.17	38.47	6.03
20	46.96	0.17	49.6	0.45	50.15	0.035

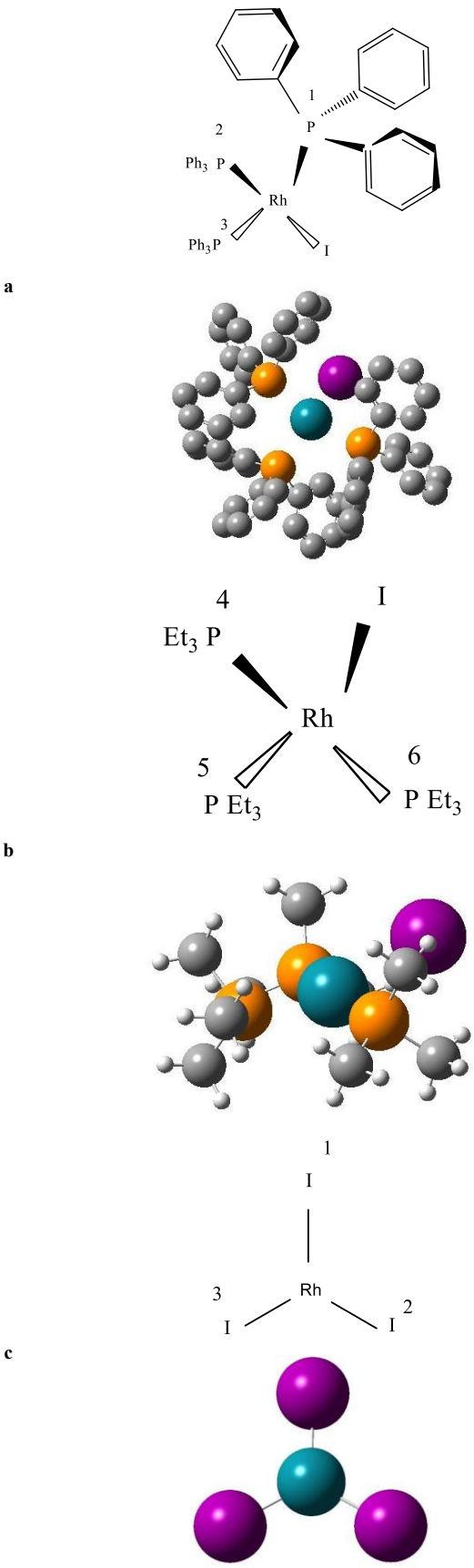
Using the $(Ph_3P)_3RhI$ catalyst resulted in the best conversion of the starting material to acetic acid after 6 hours, according to Table 5. A comparison of the data reported for AA at 6 hours shows that the $(Ph_3P)_3RhI$ catalyst leads to the formation of the minimum methyl acetate. The $(Et_3P)_3RhI$ catalyst provides the best results for AA production, even when reaction time is increased. However, using this catalyst leads to the formation of trace amounts of methyl acetate (Mac).

4. Characterization of $(Ph_3P)_3RhI$ (a), $(Et_3P)_3RhI$ (b), and RhI_3 (c) via the DFT method

Density Functional Theory (DFT) is a powerful computational method used in physics, chemistry, and materials science to explore the electronic structure of many-body systems. DFT has numerous applications for predicting molecular properties and reactivity. A literature review shows that this method is widely used to investigate the experimental data [20-24]. Also, using the DFT method, several parameters such as bond length, charge, HOMO, and LUMO energy levels can be obtained, which help in compound characterization [25,26]. Therefore, in this study, the structure, NBO analysis, HOMO, and LUMO energy levels of compounds a, b, and c were investigated.

4.1. Geometric and electronic properties

The structures of $(Ph_3P)_3RhI$, $(Et_3P)_3RhI$, and RhI_3 were optimized using Gaussian 16 with B3LYP Level. The def2-svp basis set was used to optimize the studied molecules in their ground state in order to investigate the geometrical properties such as bond lengths and dihedral angles. The optimized structures of molecules a, b, and c are shown in Scheme 3. Some their geometrical parameters are listed in Table 6. In addition, the NBO analysis, HOMO and LUMO energy levels are reported in the Table 7.



Scheme 3. General and optimized structures of a) $(Ph_3P)_3RhI$, b) $(Et_3P)_3RhI$ and c) RhI_3 compounds

The geometry of a, b, and c shows that these catalysts are irregular squares and a planner, respectively. Table 6 displays the calculated energies and electronic parameters for optimized structures.

Table 6. Selected B3lyp/def2-SVP optimized geometrical parameters obtained for a, b, and c compounds. (bond lengths and angles are given in Å and degrees, respectively)

Comp.	< P1-Rh-I	<P1-Rh-P2	<P2-Rh-P3	P1-Rh	P2-Rh	P3-Rh	Rh-I
a	91.2	98.7	98.5	2.63	2.63	2.70	2.94
	< P4-Rh-I	<P4-Rh-P5	<P5-Rh-P6	P4-Rh	P5-Rh	P6-Rh	Rh-I
b	86.0	98.1	93.4	2.57	2.53	2.57	2.94
	< I1-Rh-I2	< I1-Rh-I3	< I2-Rh-I3	I1-Rh	I2-Rh	I3-Rh	
c	119.9	119.9	120.0	2.54	2.54	2.54	

A review of the data reported in Table 6, shows that the bond lengths (Å) (P-Rh) in compound a are different because the molecular conformation is an irregular square. These data also show that the π-π, π-σ, and σ-σ interaction between P and Rh elements are differ in this conformer and confirm its geometric structure (Scheme 3 a). This trend is also observed for compound b. Steric hindrance between Phenyl-Rh, Ph-Ph, and Ph-I interactions causes a decrease in the P-Rh bond lengths in compound b compared to compound a. The P-Rh bond length in compound c is slightly longer than that of compounds a and b because the conformer of this particle is planner.

Also, the angles of P-Rh-P and P-Rh-I in compounds a and b show that these compounds are not regular squares.

Natural bond orbital analysis

Natural bond orbital (NBO) analysis can be used to describe the atom charge of a molecular system. The dipole moment, molecular polarizations, and HOMO and LUMO energy levels of molecules can be predicted by calculating their charges. Also, according to NBO analysis data, it is possible to predict the donor and acceptor atoms in a molecule [27]. Therefore, in this study, the NBO electric charges calculated for selected atoms, including P1, P2, P3, P5, Rh and I, which are important in the synthesis of the acetic acid according to the Monsanto process, are listed in Table 7.

Table 7. Natural bond orbital (NBO) analysis of the atomic charges a, b, and c compounds

Comp	P1	P2	P3	Rh	I	μ (D.B)	HOMO (eV)	LUMO (eV)
a	1.021	1.039	0.994	-0.448	-0.337	6.11	-0.168	-0.040
	P4	P5	P6	Rh	I			
b	0.988	0.1.026	0.988	-0.571	-0.440	6.86	-0.165	+0.014
c				-0.357	+0.122	0.000	-0.182	+0.007

The data reported in Table 7 show that compounds a and b are more polar than the compound c. This parameter helps increase the reaction rate in the Monsanto process because, in the first step the catalyst must dissolve in the medium under high temperature and pressure. Moreover, a review of these data, shows that the HOMO energy levels in compounds a and b are more negative than in compound c. This is useful for electron transfer from the catalyst to methyl iodide reactant in the mechanism of the Monsanto process.

Second order perturbation theory analysis of Fock matrix on NBO analysis of compounds

The interaction between filled and vacant orbitals in a system can be used to measure intermolecular delocalization. This method is called hyperconjugation. The second-order perturbation interaction energy (E (2)), can be used to quantitatively describe this parameter. Therefore, in this study, the hyperconjugative interaction energies were estimated using the second-order perturbation approach [28].

$$E(2)= \Delta E_{ij}= q_i F^2_{i,j}/\varepsilon_j-\varepsilon_i$$

Where F^2_{ij} is the Fock matrix element between the i and j NBO orbitals. The letters i and j are donor and acceptor atom or group, respectively. E(2) is the stabilization energy associated with the i-j delocalization (Table 8).

Table 8. Second order perturbation theory analysis of Fock matrix with NBO basis.

Comp.		Donor (i)	Acceptor (j) (Rh)	E (2)	E (j)-(i) a.u	F(j,i) a.u
	P2	CR	LP*	0.55	7.36	0.058
	P3	CR	LP*	1.80	7.41	0.105
a	P4	CR	LP*	0.51	7.37	0.055
	I	CR	LP*	0.78	10.04	0.080
		LP	LP*	7.05	0.40	0.047
		CR	RY*	1.31	10.13	0.105
				1.31	10.13	0.105
				1.92	10.13	0.127
b	I	LP	BD*	1.81	1.00	0.039
				1.81	1.00	0.039
				2.48	1.00	0.04
		LP	LP*	7.56	0.35	0.046
c	I1	CR	RY*	0.94	7.01	0.073
	I3	CR	RY*	0.94	7.01	0.073
	I4	CR	RY*	1.25	6.94	0.083

According to the mechanism of the Monsanto process for the synthesis of acetic acid, electron transfer of Rh to Me-I is very important. Therefore, in the Table 8, E(2) for some atoms that increase the negative charge density on the Rh center are reported. These data show that the hyperconjugative interactions in compounds a and b are greater than those in compound c, resulting in an increased negative charge on Rh atom in these two compounds. Thus, these data can confirm the different stability of these compounds in theTG method.

5. Conclusions

Two composites of the Monsanto process catalysts, $(Ph_3P)_3RhI$ and $(Et_3P)_3RhI$ were synthesized, characterized, and applied to the synthesis of acetic acid. The catalysts were characterized by ^{1}H-NMR, FT-IR, FE-SEM, TGA, EDX, XRD, and zeta potential methods. The analytical results confirmed that two composite catalysts were successfully synthesized. In this study, the solubility of two composites, an important parameter in the Monsanto process, was investigated at a CO pressure of 5 bar. According to the solubility data, the following trend was observed: $(Ph_3P)_3RhI$> $(Et_3P)_3RhI$ > RhI_3. Also, the data obtained from the synthesis of acetic acid under the same condition as the Monsanto process show that $(Et_3P)_3RhI$ exhibits better performance than the other catalysts.
Furthermore, in this project, DFT calculations were used to determine some electronic parameters important for studying the stability of these compounds. For example, the dipole moment (μ) data obtained with the DFT method show that $(Ph_3P)_3RhI$ composite is more polar than RhI_3. This result confirms their solubility. Also, according to the second-order perturbation theory analysis of Fock matrix with NBO basis, the intra electron transfer in the $(Ph_3P)_3RhI$ and $(Et_3P)RhI$ compounds is greater than in RhI_3, causing increased stability in the presence of increasing heat (TGA spectra).

Author Contributions

All authors contributed equally to the conception, preparation, and writing of this manuscript.

Conflict of Interest

The authors, while observing publication ethics in the referencing, declare the absence of interest of conflict.

Acknowledgement

The authors gratefully acknowledges the support provided by the Petroleum University of Technology of Ahvaz and Fanavaran Petrochemical company in conducting this research.

AI-Assisted

The authors retain full responsibility for the accuracy, originality, integrity, legality, and ethical compliance of all text, data, tables, figures, analyses, references, and conclusions, and have verified all AI-assisted outputs. Any fabrication, falsification, manipulation, plagiarism, copyright infringement, or other misuse of AI remains solely the responsibility of the authors and does not transfer or diminish their accountability for the published work.

References

[1] S. Medici, M. Peana, A. Pelucelli, M. A. Zoroddu, *Molecules*, 2021, **26**, 2553-2577. https://doi.org/10.3390/molecules26092553.
[2] C. Empel, S. Jana, T. Langletz, R. M. Koenigs, *Chem. Eur. J*, 2022, **28**, e202104321. https://doi.org/10.1002/chem.202104321.
[3] S. Ikeda, Y. Hanamura, H. Tada, R. Shintani, *J. Am. Chem. Soc*, 2021, **143**, 19559–19566. https://doi.org/10.1021/jacs.1c09827.
[4] J. Rankin, A. Benyei, A. Poole, D. Cole-Hamilton, *J. Chem. Soc*, Dalton Trans, 1999, 3771–3782. https://doi.org/10.1039/A905308E.
[5] Q. Qian, J. Zhang, M. Cui, B. Han, *Nat. commun*, 2016, **7**, 1-7. https://doi.org/10.1038/ncomms11481.
[6] Q. Yan, *Appl. Comput. Eng*, 2024, **61**, 216-221. https://doi.org/10.54254/2755-2721/61/20240959.
[7] P. Kalck, C. Le Berre, P. Serp, *Coord. Chem. Rev*, 2020, **402**, 2130781-58. https://doi.org/10.1016/j.ccr.2019.213078.
[8] P. J. Parulekar, S. Jadhav, *Int. J. Eng. Res. Technol*, 2025, **14(1)**, IJERTV14IS0100551-8. https://doi.org/10.5281/zenodo.18114964.
[9] A. W. Budiman, J. S. Nam, J. H. Park, R. I. Mukti, T. S. Chang, J. W. Bae, M. J. Choi, *Catal. Surv. Asia*, 2016, **20**, 173-193. http://dx.doi.org/10.1007/s10563-016-9215-9.
[10] G. J. Sunley, D. J. Watson, *Catal. Today*, 2000, **58**, 293-307. http://dx.doi.org/10.1016/S0920-5861(00)00263-7.
[11] J. H. Jones, *Platin. Met. Rev*, 2000, **44**, 94-105. http://dx.doi.org/10.1595/003214000X44394105.
[12] D. Forster, *J. Am. Chem. Soc*, 1976, **98**, 846–848. https://doi.org/10.1021/ja00419a041.
[13] P. Pal, J. Sikder, S. Roy, L. Giorno, *Chem. Eng. Process*, 2009, **48**, 1549-1559. http://dx.doi.org/10.1016/j.cep.2009.09.003.
[14] C. Schumacher, D. E. Crawford, B. Raguž, R. Glaum, S. L. James, C. Bolm, J. G. Hernández, *Chem. Commun*, 2018, **54**, 8355-8358. https://doi.org/10.1039/C8CC04487B.
[15] J. Chatt, N. P. Johnson, B. L. Shaw, *J. Chem. Soc*. 481 (1964) 2508-2513. https://doi.org/10.1039/JR9640002508.
[16] X. Che, Z. Zhang, D. Wang, W. Zhao, T. Wang, P. Zhao, G. Mu, J. Huang, F. Huang, *2D Mater*, 2020, **7**, 045034. http://dx.doi.org/10.1088/2053-1583/abb3ba.
[17] P. Li, M. Kaslan, S. H. Lee, J. Yao, Z. Gao, *Theranostics*, 2017, **7**, 789-804. http://dx.doi.org/10.7150/thno.18133.
[18] R. J. Hunter, *Academic Press*, 1981.
[19] S. Honary, F. Zahir, *Trop. J. Pharm*. Res, 2013, **12**, 255–264. http://dx.doi.org/10.4314/tjpr.v12i2.19.
[20] N. Seif, A. Farhadi, R. Badri, A. R. Kiasat, *Iran. J. Chem. Chem*. Eng, 2020, **39**, 21-33. https://doi.org/10.30492/ijcce.2019.35673.
[21] E. A. Nasab, N. Nasseh, S. Damavandi, M. Amarzadeh, M. Ghahrchi, A. Hoseinkhani, A. Alver, N. A. Khan, A. Farhadi, I. Danaee, *Environ. Sci*. Pollut. Res, 2023, **30**, 84200-84218. https://doi.org/10.1007/s11356-023-28235-z.
[22] R. Majidi, A. Farhadi, I. Danaee, N. B. Panah, D. Zarei, S. Nikmanesh, *Prog. Org. Coat*, 2023, **183**, 107803. http://dx.doi.org/10.1016/j.porgcoat.2023.107803.
[23] T. Saelee, T. Tapanya, C. Wangphon, M. Rittiruam, T. Miyake, P. Khemthong, T. Butburee, P. Limsoonthakul, S. Praserthdam, P. Praserthdam, *Fuel*, 2022, **326**, 125019, https://doi.org/10.1016/j.fuel.2022.125019.
[24] A. Farhadi, J. Noei, R. Haji Aliyari, M. Albakhtiyari, M. A. Takassi, *Res. Chem. Intermed*, 2016, **42**, 1401-1409. http://dx.doi.org/10.1007/s11164-015-2092-4.
[25] V. K. Verma, M. Guin, B. Solanki, R.C. Singh, *Mater. Today*, 2022, **49**, 3200-3204. http://dx.doi.org/10.1016/j.matpr.2020.11.887.
[26] J. R. D. Lile, S. G. Kang, Y.-A. Son, S. G. Lee, *ACS. Omega*, 2020, **5**, 15052–15062. http://dx.doi.org/10.1021/acsomega.0c00870.
[27] I. Kaur, W. Jia, R. P. Kopreski, S. Selvarasah, M. R. Dokmeci, C. Pramanik, N. E. McGruer, G. P. Miller, *J. Am. Chem. Soc*, 2008, **130**, 16274–16286. https://doi.org/10.1021/ja804515y.

S. A. Halim, A. B. El-Meligy, A. M. El-Nahas, S. H. El-Demerdash, *Sci. Rep*, 2024, **14**, 219-228. https://doi.org/10.1038/s41598-023-50660-w.